



EXPERIMENTAL INVESTIGATION OF HELICOPTER CONING / INFLOW  
DYNAMICS IN HOVER

BY

T.J. ELLENRIEDER & P.R. BRINSON

DEPARTMENT OF AEROSPACE ENGINEERING  
UNIVERSITY OF BRISTOL,  
BRISTOL, BS8 1TR, GREAT BRITAIN

TWENTIETH EUROPEAN ROTORCRAFT FORUM  
OCTOBER 4 - 7, 1994 AMSTERDAM

# EXPERIMENTAL INVESTIGATION OF HELICOPTER CONING / INFLOW DYNAMICS IN HOVER

T.J. Ellenrieder, P.R. Brinson

Department of Aerospace Engineering,

University of Bristol,

Bristol, BS8 1TR, England, U.K.

## Abstract

Coning and inflow measurements taken during collective sweeps at frequencies up to 1.5 times shaft speed on a 1.5m diameter hingeless rotor mounted on a hover stand are compared with two degree of freedom coning / inflow models. The mathematical models relating the inflow and coning degrees of freedom to the pitch inputs in collective, contained an apparent mass term to model the dynamic nature of the air flow. The theoretical models tested display less coning damping than the experimental results and reasons for this are suggested. The use of tip-loss and other lift deficiency factors to improve model fidelity are discussed. It was found that an apparent mass factor of 0.85 gives best correlation with theory.

The paper also presents the results of recent experimental studies in which the inflow frequency response was measured at various radial stations beneath the rotor disc using hot wire anemometers. These show a change in rotor inflow and thus lift distribution as the frequency of collective input excitation is increased. During collective sweeps at frequencies above shaft speed the outer regions of the blade show the largest variations in induced flow.

## List of Symbols

$v$	non-dimensional inflow degree of freedom
$v$	inflow perturbation, positive downwards
$\lambda$	non dimensional inflow
$\beta$	coning angle perturbation
$\theta$	collective pitch perturbation
$\Omega$	rotor rotational speed
$\rho$	air density
$\varepsilon$	non-dimensionalised hinge offset
$\sigma$	solidity
$\gamma$	lock number
$a$	lift curve slope
$B$	tip loss factor
$C_T$	thrust coefficient
$C^*$	lift deficiency factor
	$C^* = \frac{1}{1 + \frac{\pi\sigma}{4v_0}}$
$C_*$	thrust deficiency factor
	$C_* = \frac{1}{1 + \frac{a\sigma}{16v_0}}$
$c$	blade chord
$e$	hinge offset
$f_r^2$	flap frequency ratio
$I_\beta$	blade flapping moment of inertia
$M_\beta$	blade moment about flapping hinge
$K_\beta$	equivalent hinge spring stiffness
$k$	empirical momentum correction factor
$M_{II}$	apparent mass factor
$m$	distributed blade mass
$R$	rotor radius
$r$	radial station along blade
$C_{TLM}$	aerodynamic thrust, pitch and roll coefficients
$V_T$	momentum theory derived uniform induced flow at rotor

## **1.0 Introduction**

Despite significant progress in helicopter mathematical modelling over the past few decades, helicopter models that are typically used for flight mechanics and control work are still known to be deficient in a number of key areas. From the point of view of control and handling qualities, greatest uncertainty exists in the high frequency region where the complex dynamic and aerodynamic couplings of the rotor come into play and lack of fidelity/uncertainty in the representation of these dynamic couplings inevitably leads to conservatism in any control system design.

For a number of years, Bristol University under funding from the UK Defence Research Agency (DRA) have been developing an experimental facility that will allow the high frequency dynamics of rotor systems to be explored under laboratory conditions. One aspect of the current work which has been undertaken in conjunction with Westland Helicopters Ltd, Yeovil involves a detailed experimental investigation of rotor dynamic inflow. This paper presents the results from the first phase of this study where coupled coning/inflow theoretical models are compared with experimental data for the hover flight condition.

## **2.0 Brief Review of Inflow Theory Development**

The development of dynamic inflow theory dates back to 1950 when it was discovered that the roll and pitch damping of a helicopter was not predicted well by quasi steady theory [1]. Work in 1953 by Sissingh showed that variations in the, at that time assumed steady and uniform inflow distribution could account for the damping discrepancies. In the model by

Sissingh, the variations in inflow were assumed to be linked to the pitch and roll moments of the rotor.

In 1953 Carpenter and Fridovich [2] validated the assumption that the induced flow does not respond instantaneously to sudden pitch changes in collective, which can cause high lift transients. This was theoretically modelled by an apparent mass term equal in magnitude to that, which would be affected by an impervious disc during accelerations.

A further development was made in 1953 by Mangler and Squire [3], who found a potential pressure distribution that satisfies Laplace's equation and also gives a pressure discontinuity across the disc. Using a predetermined rotor load distribution it was shown that the induced velocity field could be calculated. Ormiston [4] tried to link load or circulation distribution, induced flow field and flapping dynamics in a closed loop form, but this became excessively complex. Ormiston and Peters [5] showed that inclusion of non-uniform inflow significantly improved the correlation with experimental flapping data of a non articulated rotor.

In 1982 Pitt and Peters [6] examined the induced flow problem from a flight dynamics point of view. They assumed that the inflow distribution could be represented assuming a fore-aft, side-to-side variation and uniform component. Again potential flow theory was used to link the degrees of freedom of the inflow distribution to the aerodynamic forces acting at the rotor hub, essentially an open loop problem. Furthermore, by extending this theory to the unsteady case (unsteady actuator disc theory) account could be taken of the apparent mass effects. The gains and time constants for the inflow distribution

degrees of freedom could thus be found for flight conditions including hover and forward flight.

Recently, a finite-state induced flow model [7] for rotors has been developed. This contains azimuth harmonics and radial shape functions to any order. The model implicitly contains dynamic inflow theory as it is also based on unsteady actuator disc theory. Correlation with experiment is good but its iterative nature makes it more suitable for the study of aeroelasticity than flight dynamics.

The number of references to the Pitt/Peters [6,8] dynamic inflow model are an indication of its wide spread use in flight mechanics models. The more sophisticated recent unsteady wake/inflow model also developed by Peters et Al [7,9] gives extremely accurate predictions of induced flow near the blade and even captures the blade passage pressure peaks. However, its iterative calculation procedures make it less useful for flight mechanics work.

### **3.0 Experimental Facility**

The rotor dynamic test facility is shown in Fig. 1. A comprehensive description of the facility is given by Brinson [10] and is briefly summarised below. The work was carried out using a four bladed 1.5m diameter rotor with rigid hub and Gottingen 436 section, 60mm chord GRP rotor blades. All tests were conducted in a simulated hover condition in the return section of the departmental large wind tunnel. The nominal rotor operating condition for the tests was 1200 RPM, giving a tip speed of 100 m/s. The datum collective setting was 11 degrees root pitch which corresponds to a rotor thrust of approximately 50lbs.

A unique feature of the rotor rig is its high performance actuation system. This comprises ac brushless electric motors connected to a conventional swash plate arrangement providing blade pitch slew rates in excess of 800 degrees/second at the blade root and a small signal bandwidth of over 50 Hz. The control of the rig is fully computerised and the system contains extensive built in safety monitoring software. Incremental shaft encoders provide accurate measurements of swashplate position and rotor blade azimuth position. The rotor system is gimballed to provide pitch and roll freedoms but for the purposes of the tests carried out for this study both gimbals were locked in the upright position.

The collective pitch was varied by +/-1.5 degrees over a frequency range extending to 30Hz (1.5 times shaft speed). Inflow data was obtained from a rake of hot wires located 15 cm below the rotor and individual blade flapping information was obtained from blade mounted strain gauges. All of the experimental data was sampled at 500Hz. The rotor speed was tightly controlled using a digital controller.

### **4.0 Data Analysis Method**

Frequency response methods were used to examine the inflow and coning behaviour of the rotor. Inputs were applied at discrete frequencies in the collective channel and the recorded data was analysed using a simple correlation procedure. Long data records were used to enhance data repeatability which was found to be excellent.

## 5.0 Theoretical Model

It has become common practice in helicopter flight mechanics models which include inflow dynamic terms to utilise a 3 Degree of Freedom (DOF) Body/Coning/Inflow representation written in state space form. If the body movement of the helicopter is restricted, as is the case on a rotor hover stand, then these reduce to a 2 DOF Coning / Inflow model with first order inflow and second order coning. The general form of the equations is given below:

$$\dot{x} = Ax + Bu,$$

$$A = \begin{bmatrix} v_v & 0 & v_\beta \\ 0 & 0 & 1 \\ \beta_v & \beta_\beta & \beta_\beta \end{bmatrix}; \quad B = \begin{bmatrix} v_\theta \\ 0 \\ \beta_\theta \end{bmatrix}$$

$$x = \begin{bmatrix} v & \beta & \dot{\beta} \end{bmatrix},$$

$$u = \theta.$$

This relatively simple representation has the advantage that it may readily be incorporated in models which require real-time computation and can be analysed with relative ease. The derivation relies on three steps common to both of the models that will be discussed. Firstly, an expression relating the inflow to the thrust is obtained, secondly an expression for the thrust perturbations in terms of inflow and coning using blade element theory is found. Lastly equations describing the behaviour of the blades are required.

### 5.1 Coning / Inflow Theoretical Models

Results are presented based upon comparisons with just two coupled coning / inflow models. Both models use the widely accepted Pitt & Peters [8] inflow formulation. Classical blade element theory is used to relate the rotor thrust to blade

pitch perturbations, local induced velocity and blade flapping. Model A is based on the formulation developed by Chen [11] and Houston [12], but has been modified to include an offset hinge representation with spring restraint, root cut-out and tip loss factors. The structure of the resulting model in state space formulation is given below:

$$\dot{x} = Ax + Bu$$

$$A = \begin{bmatrix} -\frac{4\Omega}{M_{11}}\left(\frac{C_t}{k^2}\lambda_0 + \frac{\alpha\sigma}{16}(B^2 - C^2)\right) & 0 & -\frac{4\Omega R}{3M_{11}}\left(\frac{C_t}{k}\lambda_0 + \frac{\alpha\sigma}{8}(B^2 - C^2)\right) \\ 0 & 0 & \frac{1}{8} \\ -\frac{\Omega\gamma}{2R}\left(\frac{1}{3} - \frac{\epsilon}{2}\right)C^* & -\Omega^2 f_A & -\Omega\gamma\left(\frac{1}{8} - \frac{\epsilon}{3} + \frac{\epsilon^2}{4}\right)C^* \end{bmatrix}$$

$$B = \begin{bmatrix} \frac{4\Omega^2 R \alpha v}{3M_{11} 8}(B^2 - C^2) \\ 0 \\ \frac{\Omega^2 \gamma}{8}\left(1 - \frac{4}{3}\epsilon\right)C^* \end{bmatrix}$$

$$x = \begin{bmatrix} v & \beta & \dot{\beta} \end{bmatrix}; u = \theta$$

Model B introduces tip loss factors in the flapping equation, but discards the lift deficiency factor in the flapping equation. The inclusion of a lift deficiency factor in the flapping equation in addition to a thrust deficiency factor in the blade element formulation is difficult to justify using physical arguments. The fact that a lift deficiency factor did improve correlation with flight test data during previous experimental work using the PUMA [13] is probably due to the fact that its numerical effect is similar to that of the tip loss factor. The formulation for the offset hinge in the flapping equation of model B is based on Johnson [14] and contains the hinge offset terms to an higher order than that of Chen [11].

The structure of the resulting model B in state space formulation is given below:

$$\dot{x} = Ax + Bu$$

$$A = \begin{bmatrix} -\frac{4\Omega}{M_{11}} \left( \frac{C_t}{k^2} \lambda_0 + \frac{a\sigma}{16} (B^2 - C^2) \right) & 0 & -\frac{4\Omega R}{3M_{11}} \left( \frac{C_t}{k} \lambda_0 + \frac{a\sigma}{8} (B^2 - C^2) \right) \\ 0 & 0 & 0 \\ \Omega \frac{\gamma}{6R} \left( \frac{3}{1-\varepsilon} \left( \frac{B^3}{3} - \frac{\varepsilon B^2}{2} + \frac{\varepsilon^3}{6} \right) \right) - \Omega^2 f_s & -\frac{\Omega \gamma}{8} \frac{4}{(1-\varepsilon)^2} \left( \frac{B^4}{4} - \frac{2\varepsilon B^3}{3} + \frac{\varepsilon^2 B^2}{2} - \frac{\varepsilon^4}{12} \right) & 0 \end{bmatrix}$$

$$B = \begin{bmatrix} \frac{4\Omega^2 R a \sigma}{3M_{11} 8} (B^2 - C^2) \\ 0 \\ \Omega^2 \frac{\gamma}{8} \left( \frac{4}{1-\varepsilon} \left( \frac{B^4}{4} - \frac{\varepsilon B^3}{3} + \frac{\varepsilon^4}{12} \right) \right) \end{bmatrix};$$

$$x = [\nu; \beta; \dot{\beta}]; u = \theta$$

Both models were validated using the results produced by Chen and Hindson [11] with appropriate values for rotor speed, lock number and rotor radius and with the tip loss, lift deficiency and thrust deficiency factors set to unity whilst hinge offset or rut cut out were set to zero. The results in Chen's report could thus be reproduced.

## 6.0 Comparison of Coning/Inflow Models with Experimental Data

In this section the experimentally determined coning and inflow frequency responses will be compared with the results obtain from the theoretical models. The rotor was modelled assuming a offset hinge at 28% of the blade span and spring stiffness to provide the correct flap frequency ratio. The location of the equivalent offset hinge was determined from the mode shape of the deflected blade. The datum value of the apparent mass was taken to be 0.85 and the tip loss and lift deficiencies values where chosen in accordance with the appropriate thrust and mean induced flow values.

A typical set of experimental data is shown in Fig 2. These data have been averaged

over three runs and the one standard deviation confidence interval is shown. Fig. 2 clearly shows that the data repeatability is excellent. The very slight deterioration in repeatability at low frequency is due to recirculation effects within the tunnel. At frequencies above 20 Hz the signal to noise ratio of the inflow data is poor and should therefore be treated with some caution. Despite the poor signal to noise ratio on the high frequency inflow data, the results have been found to be very repeatable. The data has all been corrected for actuation lag, which at 30 Hz is approximately 20 degrees. Additionally, the inflow data which was taken some 15 cm below the rotor disc has been corrected for wake contraction and wake transport delay [15]. The transport delay correction allows for the time that a disturbance takes to travel from the rotor disc to the hot wire measurement point. The data set depicted in Fig. 2 is taken from a hot wire measurement station at 57% blade span.

Fig 3 compares the frequency responses obtained from models A and B with the experimental data. It can be seen that model B captures the low frequency coning gain very well, but the magnitude of the coning resonant peak is over predicted by 5 dB. Model A under estimates the low

frequency coning gain and similarly underestimates the damping of the coning mode.

The small amount of phase lead predicted by both models at low frequency is not reproduced in the experimental data and consistent with the underestimation of coning damping, both models exhibit steeper phase characteristics in the vicinity of the coning resonance than that apparent in the experimental data.

The low frequency inflow response is again best captured by model B. At higher frequencies the inflow gain falls off rapidly and this behaviour is not matched by either theoretical model. Consistent with the underprediction of low frequency coning gain, model A also underestimates the low frequency inflow gain. There is no difference in the inflow formulation contained in both models, and this highlights the strong coupling between the coning and inflow low frequency behaviour. A slight recovery in the high frequency inflow gain shown in Fig. 2b, although in an area where the signal to noise ratio is poor, is consistently apparent in the experimental data but not reproduced by either of the mathematical models. The inflow phase is very well captured by both models.

### **6.1 Effect of Changes in the Apparent Mass Term**

The value of the apparent mass factor has been studied previously [6,2]. The theoretical value initially suggested by Pitt and Peters [6], for a corrected pressure distribution, is 0.54 and may be contrasted with the value of 0.85 proposed by Carpenter and Fridovich [2]. Previous studies of the PUMA hover dynamics [12,13] have suggested that an apparent mass term of 0.85 gives better results.

The effect of variation of the apparent mass term is shown in Fig 3. As would be expected the primary effect of the apparent mass term is on the inflow response and not the coning response. The lowest value of  $M_{11}$  studied causes the coning resonant peak to increase by approximately 1.5 dB. Variation in apparent mass causes no appreciable change in the coning phase. Lowering the apparent mass term strengthens the coupling between the inflow and coning freedoms.

The primary effect of the apparent mass factor is to change the bandwidth of the inflow response and values of  $M_{11}=0.54$  and below cause a slight resonant peak to appear in the theoretical results at just over 20 Hz. This increases as  $M_{11}$  is decreased. As the apparent mass factor is increased to 0.85, which is the value originally suggested by Carpenter and Fridovich, the inflow gain and phase start to roll off more rapidly, providing better agreement with the experimental data. From this it can be concluded that a larger proportion of the surrounding air is being influenced by the pitch perturbations than that suggested using a corrected pressure distribution. Using an apparent mass term of  $M_{11}=0.85$  the theoretical model remains deficient in characterising the coning damping and fails to capture the steep reduction in inflow gain at 10Hz. The latter of these two apparent deficiencies of the theoretical model is probably more serious because of the implications for 'tight' heave axis hover control.

### **6.2 Model Response with Increased Coning Damping**

The coning damping is primarily determined by the coning rate derivative with a contribution from the apparent mass term and it is clear that there is a deficiency in the strength of the coning rate derivative

in the theoretical model. The structure of the coning damping derivative is given below and the factor B is suggested by Johnson [14] to represent blade tip loss effects.

$$\beta_{\dot{\beta}} = \frac{-\Omega\gamma}{8} \frac{4}{(1-\varepsilon)^2} \left( \frac{B^4}{4} - \frac{2\varepsilon B^3}{3} + \frac{\varepsilon^2 B^2}{2} - \frac{\varepsilon^4}{12} \right)$$

In what follows, an argument for excluding the tip loss factor in the coning damping derivative will be developed and to justify the approach, the derivation of the flapping equation must be examined in some detail. For a complete derivation the reader is referred to Johnson [14]. In small perturbation form and using non-dimensional quantities the flapping equation is given by:

$$\ddot{\beta} + f_R \dot{\beta} = \gamma M_F; \quad M_F = \int_{\varepsilon}^1 \eta \frac{F_Z}{ac} dr$$

where  $F_Z$  is given by,

$$\frac{F_Z}{ac} = 0.5(U_T^2 \theta - U_P U_T)$$

$U_P$  and  $U_T$  are the normalised air velocities at the blade section perpendicular and tangential to the disk plane, respectively. The rigid rotation about a flap hinge is represented by  $\eta$ , which is normalised in such a way, that for no hinge offset  $\eta = r$  and then the deflection of the blade is given by  $\beta\eta$ .

$$U_P = \lambda + \eta\dot{\beta} \quad \text{and} \quad U_T = r;$$

The expression for  $M_F$  is then integrated over the disc and the following result is obtain from Johnson p[14].

$$M_F = \frac{1}{8} C_2 \theta_0 - \frac{1}{6} C_1 \lambda - \frac{1}{8} D_1 \dot{\beta}$$

The expressions for the constants C1, C2 and D1 are given by Johnson and involve an integration from the location of the

assumed offset hinge to the blade tip, i.e. from  $\varepsilon$  to the blade tip. To include the effect of tip loss, Johnson suggests that the integrals are evaluated from  $\varepsilon$  to B.

The tip loss factor is used to approximate the decrease in lift over a finite distance at the blade tip. Over the length of the blade outside the tip loss region the lift and thus inflow is assumed to be zero. It can be argued however that the air velocity perpendicular to the blade outside of the tip loss region due to the flapping motion is still present and acts to damp the flapping motion of the blade. The expression for  $U_P$  is then given by:

$$U_P = \begin{cases} \lambda + \eta\dot{\beta}; & r \leq B \\ \eta\dot{\beta}; & r > B \end{cases}$$

The limits of the integral for C1 are thus  $\varepsilon$  to 1, whilst the other integrals are only evaluated up to the tip loss region. The modified coning damping derivative is thus given by:

$$\beta_{\dot{\beta}} = \frac{-\Omega\gamma}{8} \frac{4}{(1-\varepsilon)^2} \left( \frac{1}{4} - \frac{2\varepsilon}{3} + \frac{\varepsilon^2}{2} - \frac{\varepsilon^4}{12} \right)$$

Clearly, the effect of this modification to the flapping equation is to increase the coning rate derivative, and the result is depicted in Fig 5. Only the coning gain and inflow gain responses are shown as the effect on the phase was found to be minimal. It can be seen that the resonant coning peak has been reduced by approximately 2 dB for all cases of apparent mass considered. Significantly however, although the effect on the coning response is relatively small, the increased coning damping has increased the rate at which the inflow gain rolls off. Once again, a value of 0.85 for the apparent mass provides the best agreement between the theoretical and experimental data. The effect of further increasing the coning damping derivative to match the damping

of the coning mode to the experimental data is shown in Fig 6. Here, the coning rate derivative has been increased by 3.5dB. The inflow response now shows a sharp dip in gain at the coning resonant frequency, and interestingly, also shows a slight recovery in the response at high frequency. The frequency response obtained using an apparent mass value of 0.85 gives a good overall fit to the experimental data, with the inflow gain reducing from 3 Hz onwards and this model may be used to examine the coning and inflow behaviour with reasonably good fidelity up to rotor shaft frequencies.

### **7.0 Radial Inflow Distribution**

Further work was conducted to examine the radial distribution of the inflow perturbations due to collective inputs over the same frequency range (0.5 to 30 Hz). Fig. 7 shows the gain curves of the inflow response over the radial span of the rotor blade taken 15cm below the rotor using hot wires. Fig. 8 shows the same information on a carpet plot and additionally shows the cases of 1000 rpm and 1500 rpm operating conditions.

As the frequency of the collective input is increased, the characteristic shape of the inflow distribution changes. At higher frequencies a strong peak develops in the region of 75% of the blade span.

Between 15 and 21 Hz a secondary smaller peak develops at between 20% and 40% of the rotor radius. The repeatability of these results is extremely good, the dotted line on the figure indicating the one standard deviation confidence interval over 3 consecutive runs.

These results suggest that at high frequencies the outer section of the blade produces the highest induced velocities and thus also most lift. Several effects may contribute to this result and the result is deserving of further investigation. The Reynolds number of the flow as referenced to the blade at a certain radial station varies along the span of the blade, increasing outboard. It is known that the lift characteristics of an aerofoil section vary with Reynolds number and this may be a contributory cause for the redistribution of the induced flow with frequency. Furthermore, it is also known that the dynamic lift characteristic of an aerofoil depends on the non-dimensional reduced frequency of its oscillation [16]. Again, because of the rotating nature of the blade the reduced frequency will vary with radial station, providing a further possible explanation for the redistribution of induced flow.

### **8.0 Future Work**

The current work programme includes studies using a three component laser Doppler anemometry system. These studies will enable high quality inflow data to be acquired closer to the rotor blades. A series of inflow measurements with cyclic pitch perturbations at the hover and low advance ratios is planned. The results will be correlated with theoretical models which include dynamic inflow terms.

### **9.0 Conclusions**

Lack of fidelity in the mathematical models used for flight mechanics and control studies remains one of the principle barriers to the successful introduction of full authority active control systems for helicopters. A rotor dynamic facility has been developed which provides a unique

opportunity to explore the high frequency behaviour of helicopter rotors and hence address some of the existing known model deficiencies.

The coupled coning/inflow theoretical models tested underestimate the damping of the coning mode. The magnitude of the coning damping significantly affects the character of inflow response and artificially increasing the coning damping reproduces the rapid decrease in the inflow response and subsequent slight recovery at the coning resonant frequency seen in the experimental data. A modification to the blade flapping equation has been suggested and this partially rectifies the deficiency in coning damping.

The rapid decay in inflow response at high frequency is responsible for the characteristic increase in rotor thrust which accompanies high rates of application of collective and this feature is therefore especially important in control system design studies where "tight" heave axis control is sought.

The coning/inflow model B when adjusted to strengthen the flapping rate derivative provides a good approximation to the experimental coning and inflow frequency responses over a frequency range extending to rotor shaft speed.

The best model fit to the experimental data is obtained when an inflow apparent mass factor of 0.85 is used and this is in agreement with previous studies of the PUMA hover dynamics conducted by Houston [12,13].

Examination of the radial distribution of the inflow response has shown that the character of the inflow behaviour changes significantly with frequency and in particular, sharp peaks occur in the radial distribution as the frequency of input excitation is increased. This result highlights the complexity of the structure of the wake and is deserving of further detailed study.

## References

- 1 Sissingh G.J., 1951  
**The Effect of induced velocity on Helicopter Rotor Damping in Pitch And Roll**  
RAE No. 24 ; November 1951
- 2 Carpenter P.J.& Fridovich, 1953  
**Effect of a Rapid Blade pitch increase on Thrust and Induced Velocity Response of a Full-Scale Helicopter Rotor**  
NACA TN3044
- 3 Mangler K.W.; H.B. Squire, 1953  
**The Induced Velocity Field of a Rotor**  
A.R.C. R. & M. No. 2642
- 4 Ormiston R.A., 1972  
**An Actuator Disk theory for Rotor wake Induced Velocities**  
AGARD Specialists meeting on the Aerodynamics of Rotary wings France 1972
- 5 Ormiston R.A. & Peters D.A., 1972  
**Hingeless Helicopter Rotor Response with Non-Uniform Inflow and Elastic Blade Bending**  
Journal of Aircraft Vol. 9, no. 10; October 1972
- 6 Pitt D.M., Peters D. A., 1983  
**Rotor Dynamic Inflow Derivatives and Time constants from various inflow models**  
9th European Rotorcraft Forum, 1983.

- 7 Peters D.A. , Boyd D.D. , He C.J., 1987  
**Finite-State Induced-Flow Model for Rotors in Hover and Forward Flight**  
43rd Annual Forum of the American Helicopter Society, 1987.
- 8 Pitt D.M. & Peters D.A., 1981  
**Theoretical Prediction of dynamic Inflow Derivatives**  
Vertica Vol15 1981; pp 21 -34
- 9 Su A. , Yoo K.M. , Peters D.A., 1992  
**Extension and Validation of an Unsteady wake Model for Rotors**  
Journal of Aircraft, Vol. 29, No. 3
- 10 Brinson P.R. 1991  
**Experimental Investigation of Coupled Helicopter Rotor/Body Control**  
17th European Rotorcraft Forum
- 11 Chen R.T., Hindson W.S 1987  
**Influence of Dynamic Inflow on the Helicopter Vertical Response**  
Vertica Vol. 11 No 1/2, pp. 77-91; 1987
- 12 Houston S.S 1989  
**Identification of Factors Influencing Rotorcraft Heave Axis Damping and Control Sensitivity in the Hover**  
RAE Technical Report 88067, Jan. 1989
- 13 Houston S.S & Tartellin P.C., 1989  
**Theoretical and Experimental Correlation of helicopter Aeromechanics in Hover**  
RAE Tech. memo Fm 20
- 14 Johnson W., 1980  
**Helicopter Theory**  
ISBN 0-691-07917-4
- 15 Ellenrieder T.J. 1993  
**Correlation of 2 Degree of Freedom Coning / Inflow Helicopter Rotor Models with Data Obtained from a Hover Stand**  
Internal Report No. 481, Department of Aerospace, University of Bristol
- 16 Fung, Y.C.  
**An Introduction to the Theory of Aeroelasticity**  
Galcit aeronautical Series, John Wiley & Sons, Inc. 1955, Library of Congress CCN: 55-9364

## Acknowledgements

This work has been supported by Westland Helicopters Ltd, Yeovil, and their technical and financial support is gratefully acknowledged. The authors would also like to acknowledge the contribution made by the U.K. Defence Research Agency by supporting the development of the rotor rig.

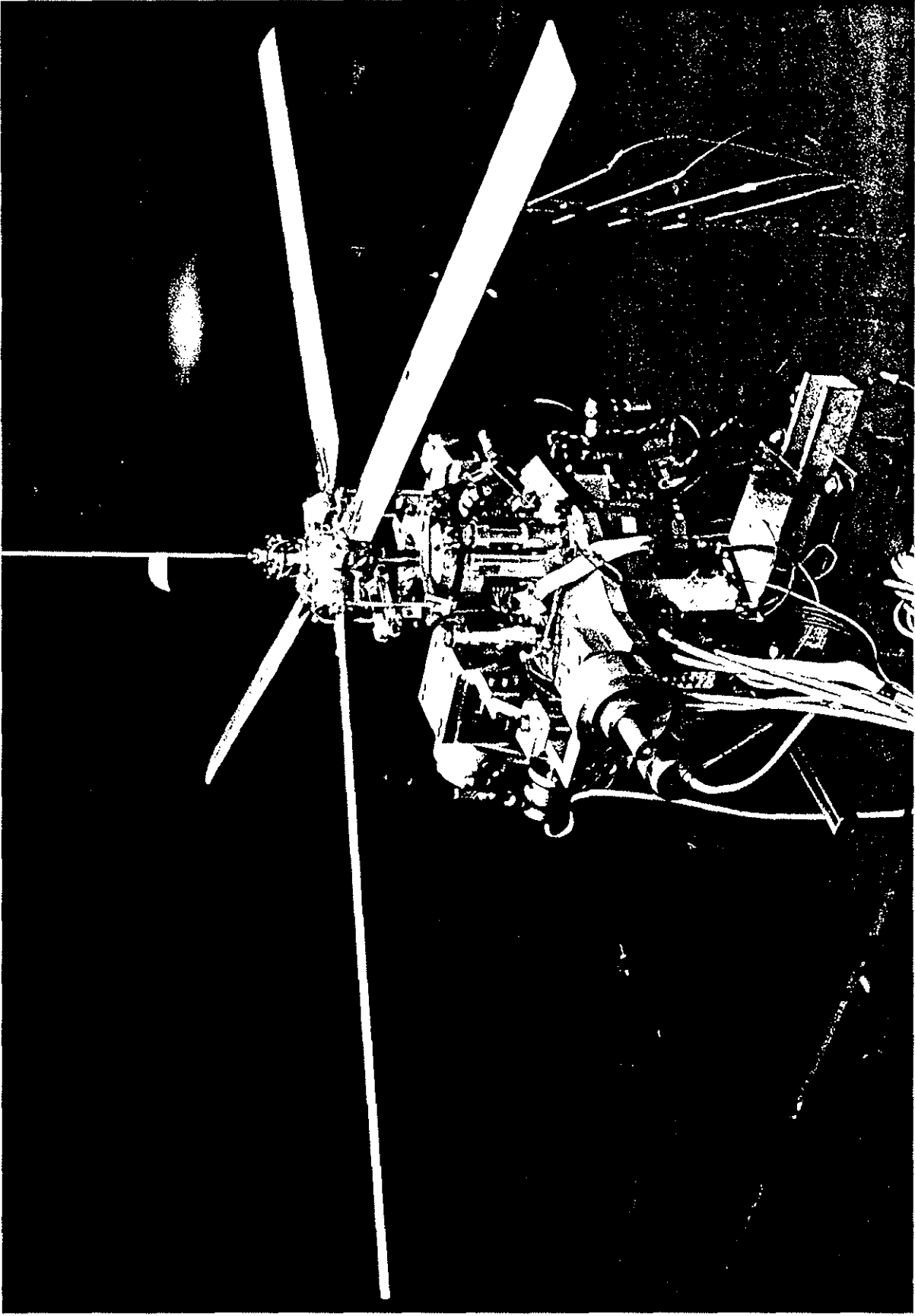


Fig 1 Dynamic Helicopter Research Rig

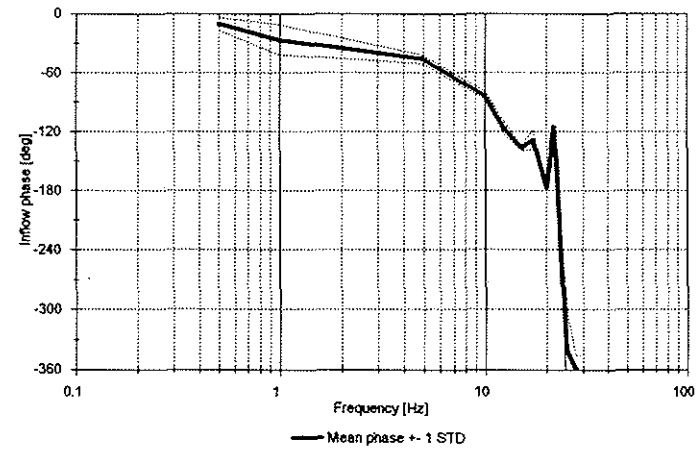
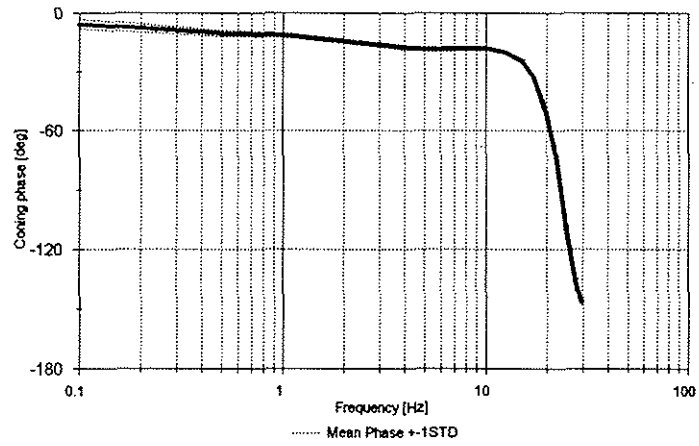
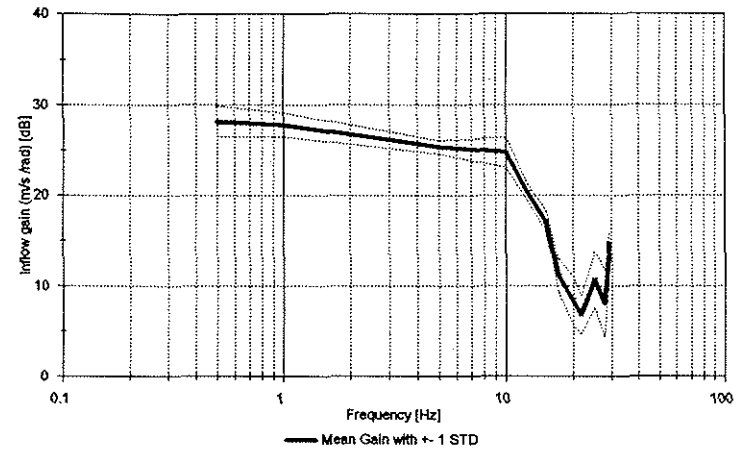
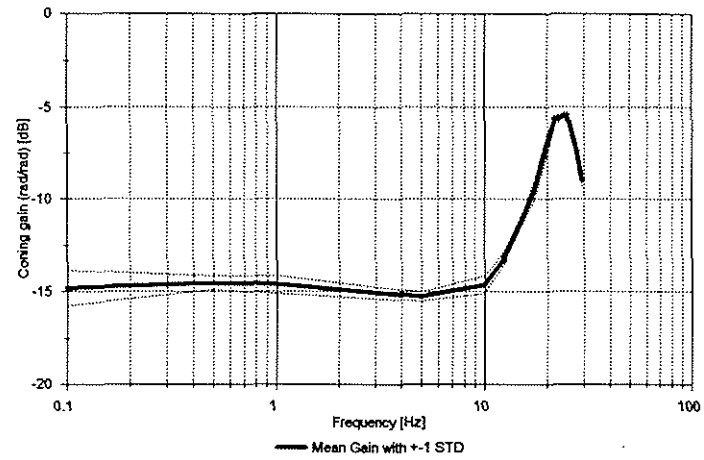


Fig 2 Experimentally Determined Coning and Inflow Dynamics at 57% Rotor Radius

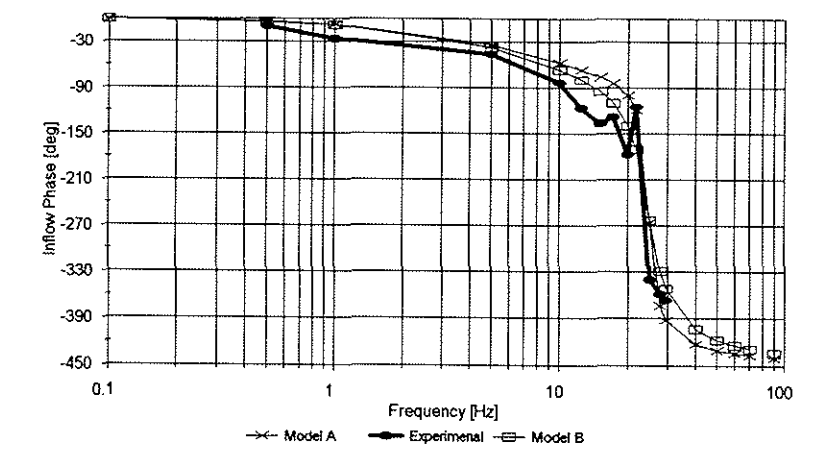
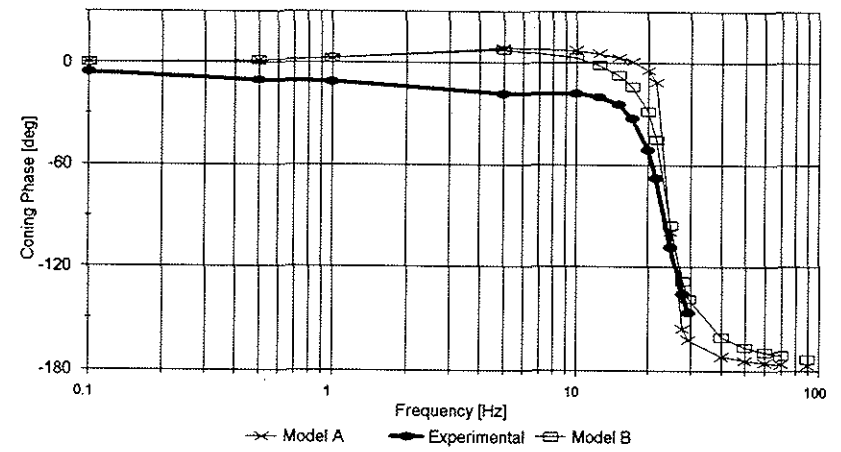
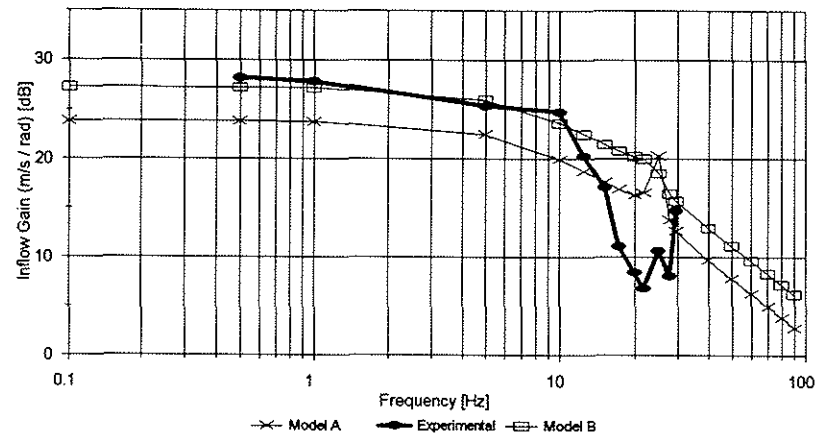
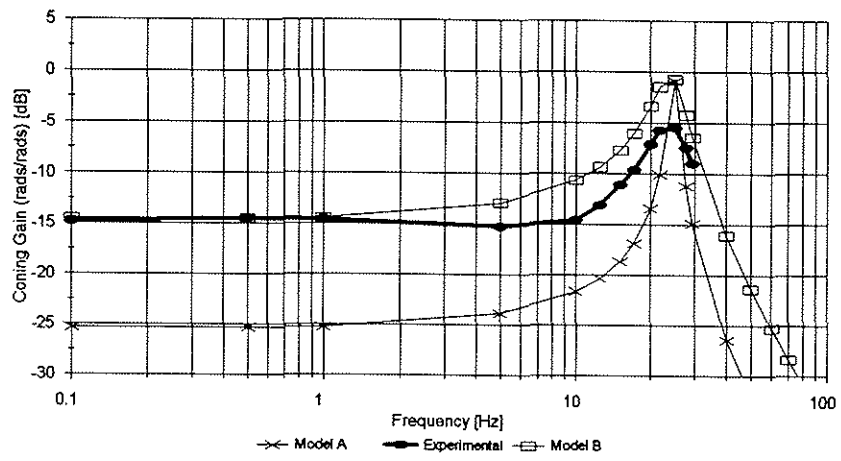


Fig 3 Correlation of Coning / Inflow Models with Experimental Data

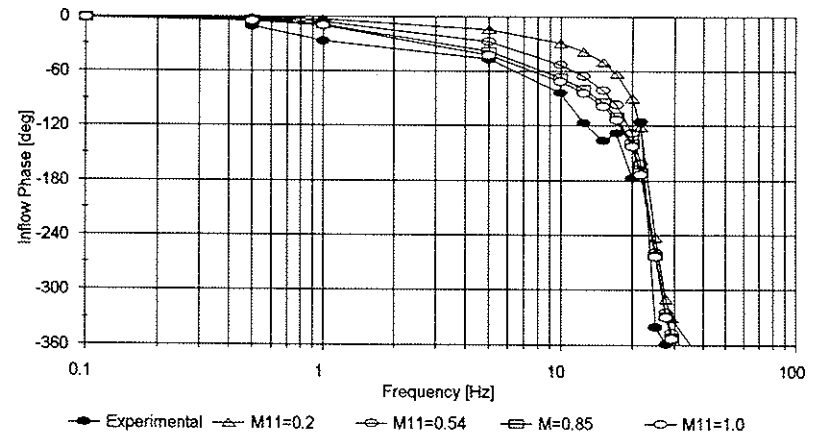
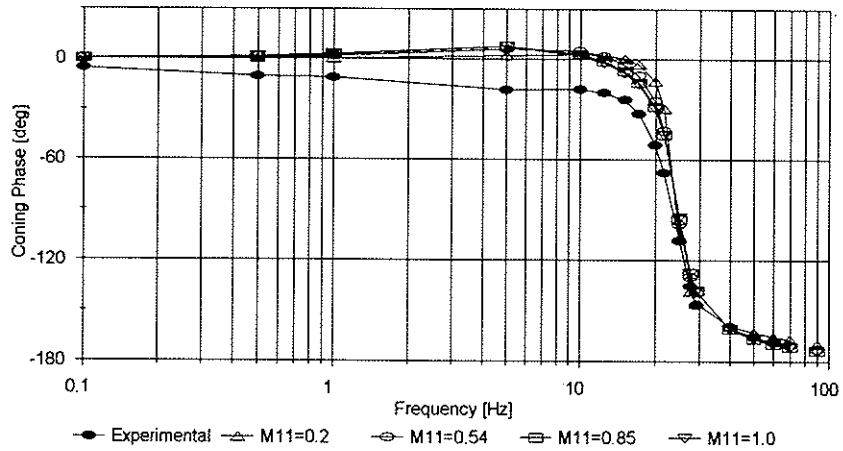
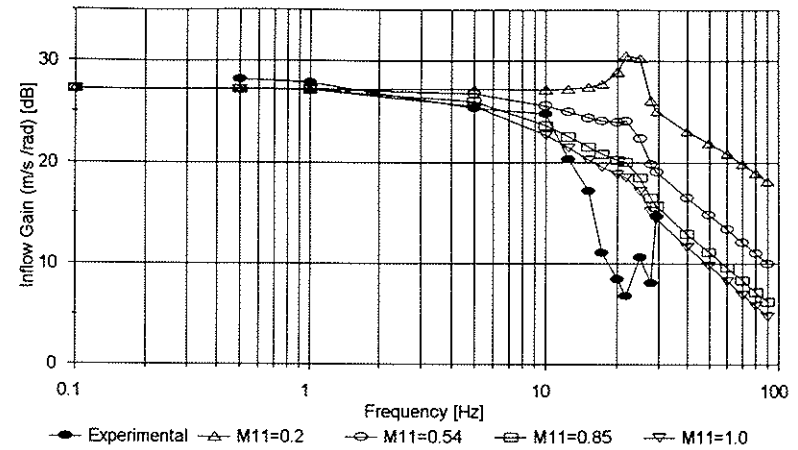
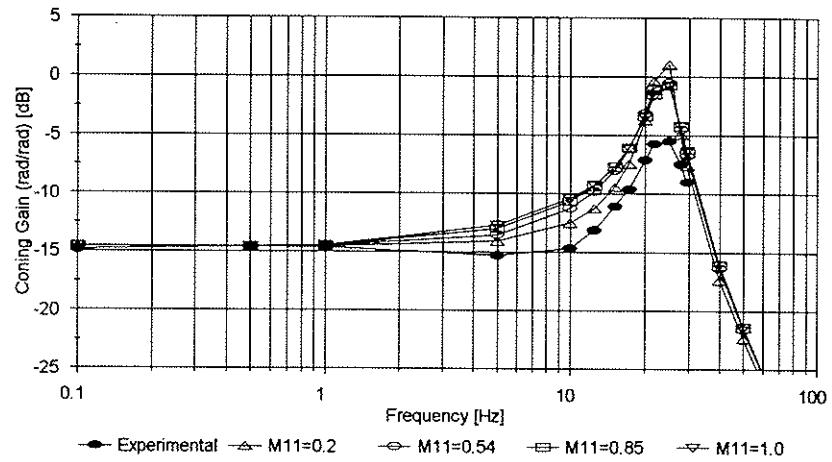


Fig 4 Effect of Apparent Mass Factor on Model B Fidelity

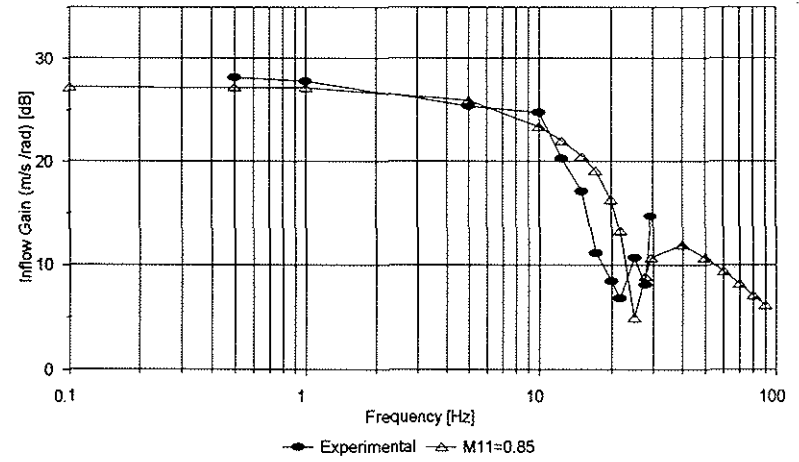
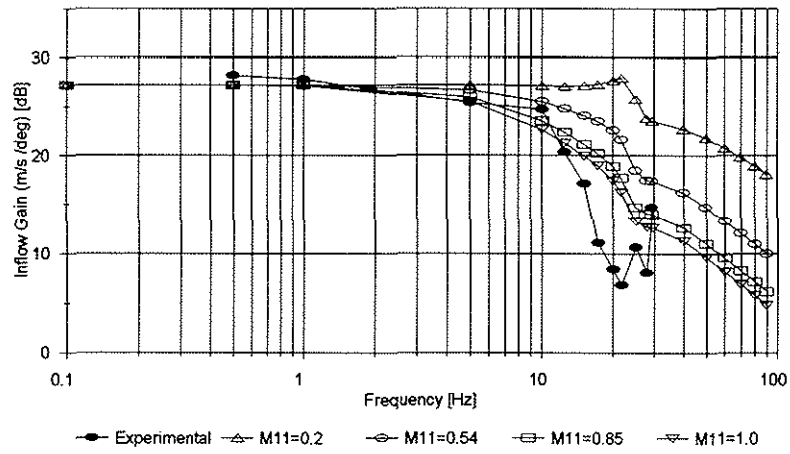
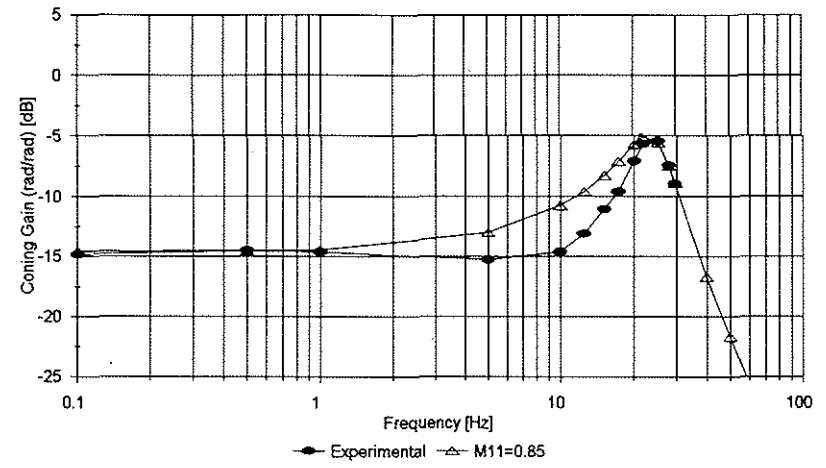
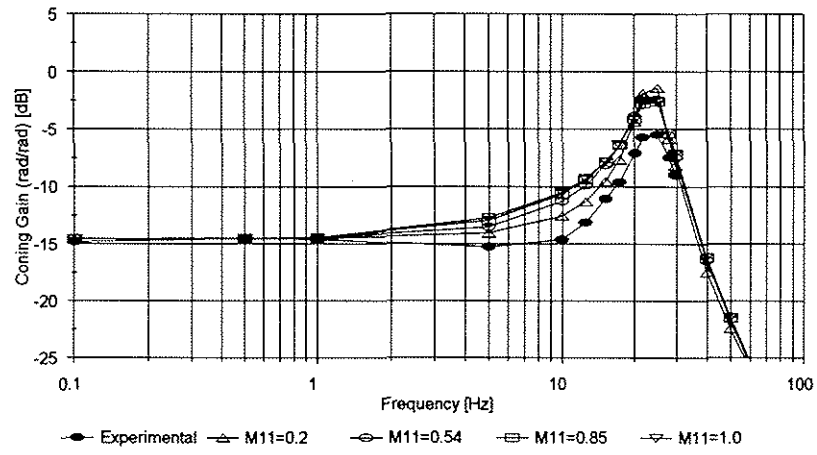


Fig 5 Effect of Increased Damping on the Fidelity of Model B

Fig 6 Effect of Artificially Increased Damping on the Correlation of Model B

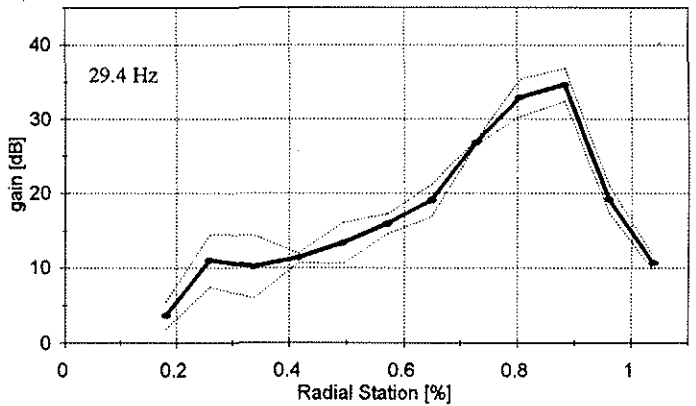
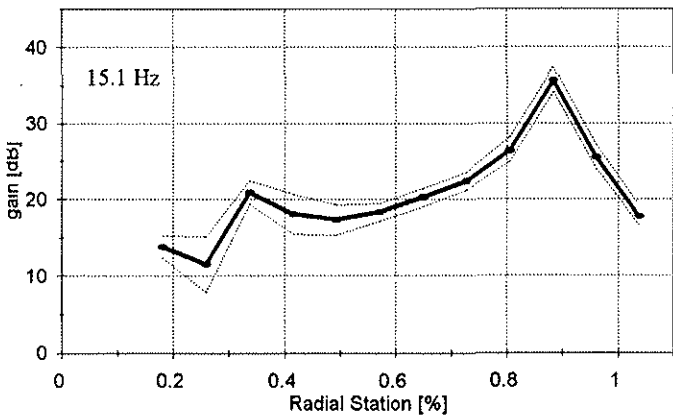
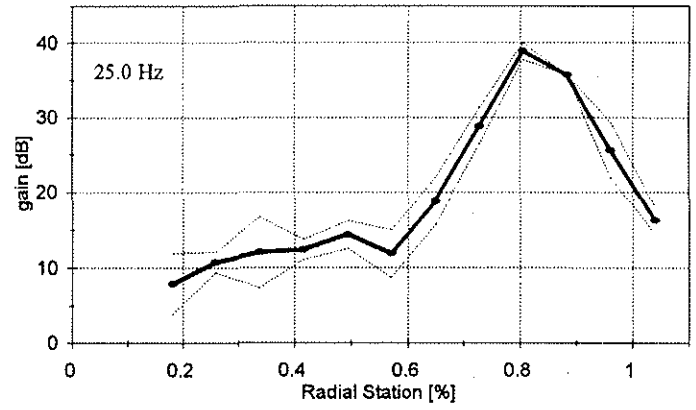
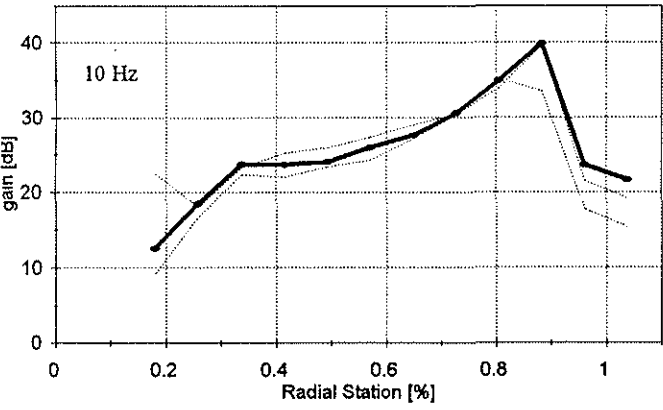
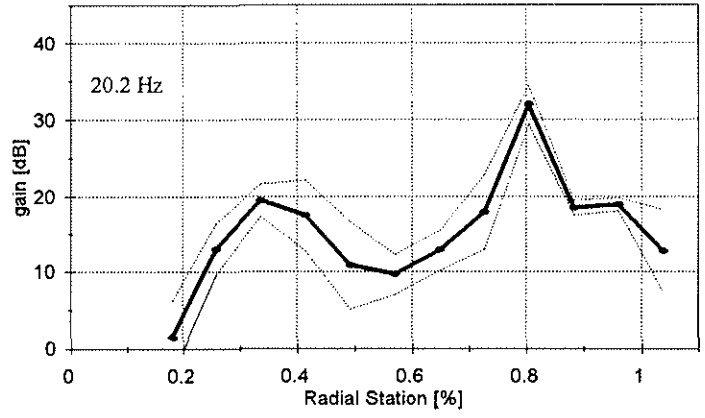
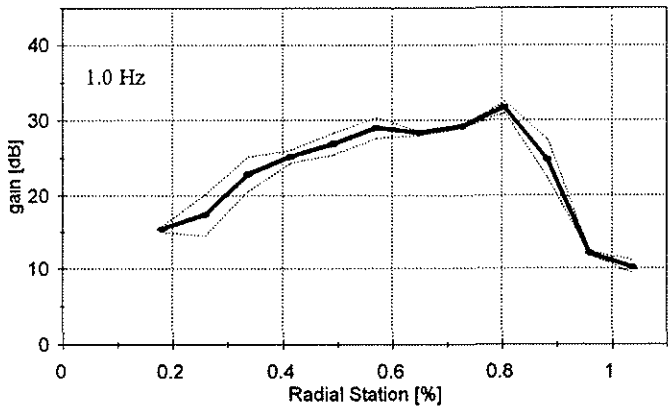
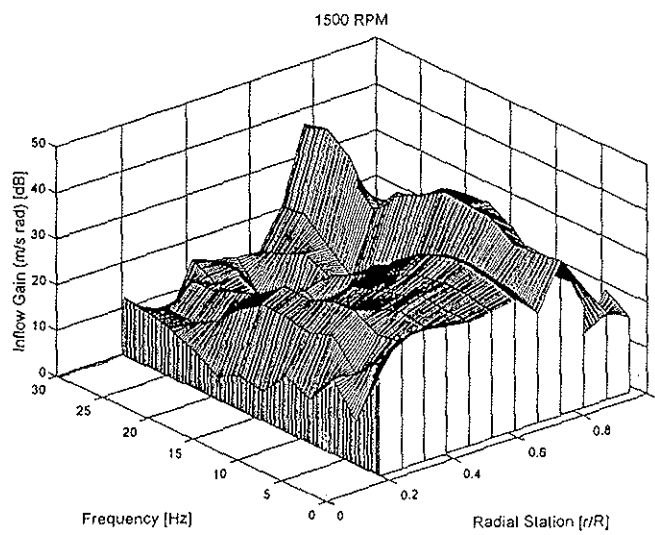
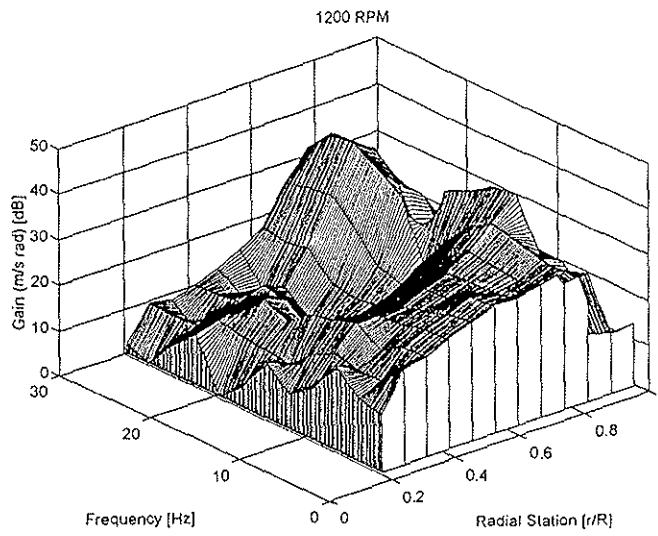
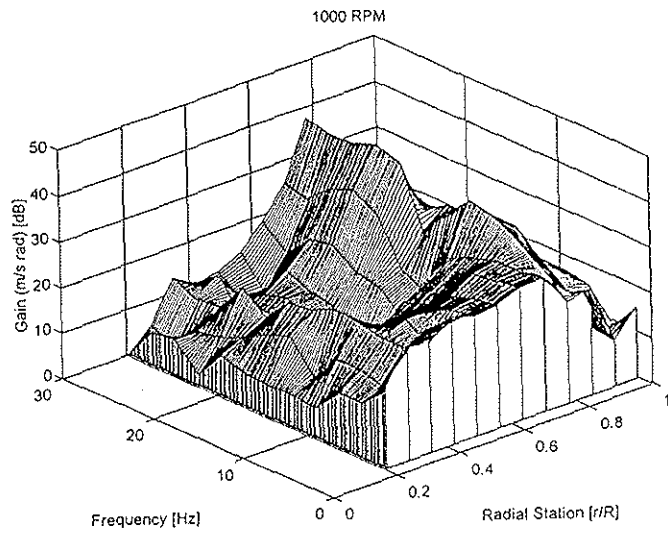


Fig. 7 Radial Variation of Dynamic Induced Velocity at an Operating Speed of 1200 RPM



**Fig 8 Induced Velocity Distribution Along the Blade Span over a Range of Frequencies at Three Rotor Speeds**